

# Targeting SARS-CoV-2 Main Protease: A Successful Story Guided by an *In Silico* Drug Repurposing Approach

Francesca Alessandra Ambrosio, Giosuè Costa,\* Isabella Romeo, Francesca Esposito, Mohammad Alkhatib, Romina Salpini, Valentina Svicher, Angela Corona, Paolo Malune, Enzo Tramontano, Francesca Ceccherini-Silberstein, Stefano Alcaro, and Anna Artese



Cite This: <https://doi.org/10.1021/acs.jcim.3c00282>



Read Online

ACCESS |



Metrics & More

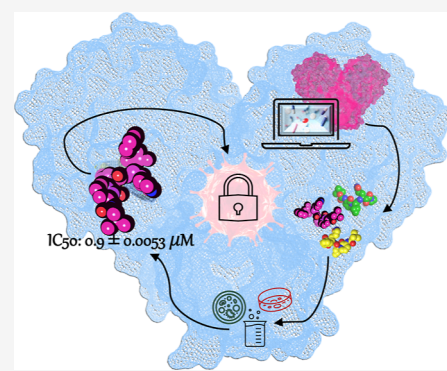


Article Recommendations



Supporting Information

**ABSTRACT:** The SARS-CoV-2 main protease ( $M^{pro}$ ) is a crucial enzyme for viral replication and has been considered an attractive drug target for the treatment of COVID-19. In this study, virtual screening techniques and *in vitro* assays were combined to identify novel  $M^{pro}$  inhibitors starting from around 8000 FDA-approved drugs. The docking analysis highlighted 17 promising best *hits*, biologically characterized in terms of their  $M^{pro}$  inhibitory activity. Among them, 7 cephalosporins and the oral anticoagulant betrixaban were able to block the enzyme activity in the micromolar range with no cytotoxic effect at the highest concentration tested. After the evaluation of the degree of conservation of  $M^{pro}$  residues involved in the binding with the studied ligands, the ligands' activity on SARS-CoV-2 replication was assessed. The ability of betrixaban to affect SARS-CoV-2 replication associated to its antithrombotic effect could pave the way for its possible use in the treatment of hospitalized COVID-19 patients.



## INTRODUCTION

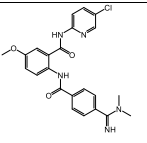
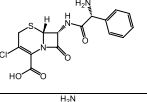
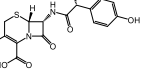
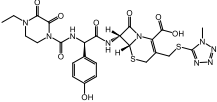
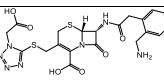
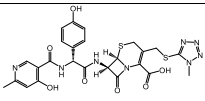
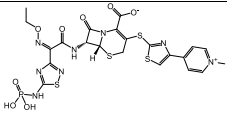
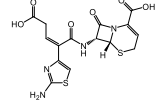
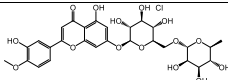
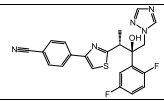
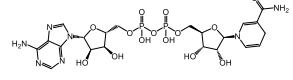
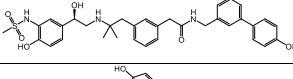
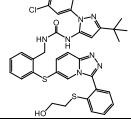
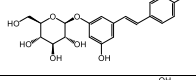
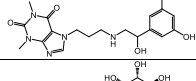
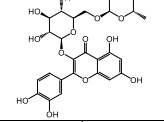
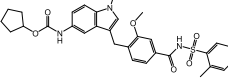
In December 2019, a novel virus defined severe acute respiratory syndrome coronavirus 2 (SARS-CoV-2) spread rapidly around the world and caused the outbreak of coronavirus infectious disease 2019 (COVID-19). As of January 2023, the number of confirmed infections had reached nearly 630 million causing more than six million fatalities.<sup>1</sup> SARS-CoV-2 is a positive-strand RNA enveloped beta-coronavirus, and similar to severe acute respiratory syndrome coronavirus (SARS-CoV) and Middle East respiratory syndrome coronavirus (MERS-CoV), contains a genome that encodes non-structural proteins (nsp's) featuring main protease ( $M^{pro}$ , also known as 3-chymotrypsin-like protease, 3CL $^{pro}$ ), papain-like protease (PL $^{pro}$ ), helicase (nsp13), and RNA-dependent RNA polymerase (RdRp).<sup>2,3</sup> Among them,  $M^{pro}$ , resulting from the maturation of at least 12 nsp's,<sup>4</sup> is a crucial enzyme in the viral life cycle and could be selectively inhibited since its structure and substrate are different from human proteases.<sup>5,6</sup> Structurally, SARS-CoV-2  $M^{pro}$  contains three structural domains connected by flexible loops. Domains I and II are  $\beta$ -barrel domains and include the catalytic active site region, whereas domain III is an  $\alpha$ -helical domain required for dimerization.<sup>7</sup> The catalytic dyad of the active site is represented by a cysteine residue (Cys145) that acts as a nucleophile and a histidine residue (His41) that acts as the general acid or base, aiming at the cleavage of the polyprotein 1a (pp1a) and 1ab (pp1ab) translated from the viral RNA at 16 different positions to produce various nsp's engaged in

stopping the viral assembly process in the replication cycle.<sup>8</sup> Although all enzymes that cooperate to the viral replication of SARS-CoV-2 are possible druggable targets, main efforts were focused on  $M^{pro}$  due to its essential role in the proteolytic process.<sup>9,10</sup>

To achieve this goal, multiple drug discovery strategies, such as virtual screening, drug repurposing, high-throughput screening (HTS), and structure-based drug design, were employed to identify promising  $M^{pro}$  inhibitors against SARS-CoV-2.<sup>5,6,11–14</sup> Thereby, numerous marketed drugs and other structurally diverse synthetic and natural compounds turned out to be efficacious inhibitors of SARS-CoV-2  $M^{pro}$ . For example, multiple lead  $M^{pro}$  inhibitors, such as boceprevir,<sup>10</sup> an HCV serine protease inhibitor,<sup>15</sup> SDZ-224015,<sup>16</sup> an investigational caspase-1 inhibitor,<sup>17</sup> and GC-376,<sup>10</sup> a cysteine protease covalent inhibitor against picornaviruses, noroviruses, and coronaviruses,<sup>18</sup> arose from efficient high-throughput (HTS) inhibition experiments. Similarly, some  $M^{pro}$  inhibitors with a high *in vitro* and *in vivo* potency, such as PF-00835231 and PF-07304814,<sup>19</sup> N3,<sup>20</sup> and the  $\alpha$ -ketoamide<sup>6</sup> have been highlighted by applying *de*

Received: February 25, 2023

**Table 1. DrugBank ID Code, Name, 2D Representation, and Glide Average Docking Scores (*D*-Scores) of the Best 17 Compounds Identified by the Structure-Based Virtual Screening Approach**

N°	DrugBank ID	Name	2D structure	Average <i>D</i> -score <sup>a</sup>
1	DB12364	Betrixaban		-8.14
2	DB00833	Cefaclor		-7.96
3	DB01140	Cefadroxil		-7.52
4	DB01329	Cefoperazone		-8.59
5	DB00923	Ceforamide		-7.58
6	DB00430	Cefpiramide sodium		-8.64
7	DB06590	Ceftaroline fosamil		-7.64
8	DB01415	Ceftibuten dihydrate		-7.50
9	DB08995	Diosmin		-8.52
10	DB11633	Isavuconazole		-7.74
11	DB00157	NADH		-8.45
12	DB11871	PF-00610355		-8.41
13	DB12138	PF-03715455		-8.87
14	DB11263	Polydatin		-8.02
15	DB12846	Reproterol		-8.78
16	DB01698	Rutin		-8.58
17	DB00549	Zafirlukast		-7.67

<sup>a</sup>*D*-score values are expressed in kcal/mol.

*de novo* development programs, now faster and more easily feasible thanks to the availability of detailed M<sup>Pro</sup> structural information as well as of structure–activity relationship (SAR) studies with reported SARS-CoV and MERS-CoV M<sup>Pro</sup> inhibitors.<sup>21–23</sup>

To date, the only compound in clinical use as M<sup>Pro</sup> inhibitor is PF-07321332 (nirmatrelvir),<sup>24</sup> a reversible covalent inhibitor orally administered and co-formulated with ritonavir (known as Paxlovid). It results in roughly a 90% protection against severe COVID-19 and hospitalization<sup>25</sup> and, even in presence of evolutionary mutations at the M<sup>Pro</sup>-gene, its antiviral potency does not seem to be compromised.<sup>26</sup> Despite the above-mentioned success stories of *de novo* development, the significant time and costs required are detrimental for keeping up with the pandemic emergency of these last three years. Thus, the drug repurposing of approved or investigational drugs still represents a practical strategy for the fast identification, characterization, and development of antiviral treatments owing to the availability of existing detailed data on drug medicinal chemistry, human pharmacology, and toxicology.<sup>27</sup> Indeed, the antivirals remdesivir (a monophosphoramidate prodrug of the nucleoside GS-441524, known to treat Ebola virus infections)<sup>28</sup> and molnupiravir (a prodrug of the nucleoside analogue  $\beta$ -D-N4-hydroxycytidine originally developed against different RNA viruses such as influenza)<sup>29</sup> are investigated as SARS-CoV-2 RNA-dependent RNA polymer-

ase (RdRp) inhibitors and the only ones in clinical use. These broad-spectrum antiviral drugs are able to reduce the progression of COVID-19 and related clinical symptoms along with a substantial decrease in recovery time.<sup>30,31</sup>

Nevertheless, efficient treatments are still required for people who are unvaccinated or immunocompromised patients who may not fully respond to vaccination and for crossing the vaccine escape induced by the occurrence of viral mutations.<sup>32</sup>

Herein, we applied an *in silico* drug repurposing approach toward M<sup>Pro</sup> enzyme by screening more than 8000 approved and investigational Food and Drug Administration (FDA) compounds and then we experimentally validated the most promising repurposed drugs. Given the crucial role of M<sup>Pro</sup> in coronavirus replication, a sequence conservation analysis was carried out to characterize the degree of conservation of the enzyme and to get insights on the conservation of the residues involved in the binding with the identified compounds.

Among 17 selected molecules, 8 were found to effectively inhibit SARS-CoV-2 M<sup>Pro</sup> activity and 3 of them in a low micromolar range. Particularly, the most potent compound, the oral anticoagulant betrixaban, was also able to block the viral replication in the micromolar range.

## RESULTS AND DISCUSSION

***In Silico* Drug Repurposing.** Starting from the M<sup>Pro</sup> crystal structure deposited in the Protein Data Bank (PDB)

with the PDB code 6Y2G, we performed molecular dynamics simulations (MDs) in order to explore all the possible conformational changes into M<sup>Pro</sup> binding site. The whole trajectory was then clustered with respect to the root mean square deviation (RMSD), thus obtaining four representative structures. With the aim of identifying promising inhibitors, we applied a drug repurposing approach by means of a structure-based virtual screening of the FDA-approved and investigational drugs against the four generated clusters of SARS-CoV-2 M<sup>Pro</sup>. According to their average Glide docking score (*D*-score) ranking, obtained as consensus value of the four used clusters, we finally selected the 17 best *hits* reported in Table 1 (for details, see the experimental section).

**Effect of Candidate Drugs on SARS-CoV-2 M<sup>Pro</sup> Activity in FRET Assay.** The 17 best candidates were purchased and then tested for their inhibitory properties against SARS-CoV-2 M<sup>Pro</sup> in a biochemical assay. While a part of the compounds resulted inactive ( $IC_{50} > 30 \mu M$ , namely, the highest tested concentration in our assay), we found that some of them were able to inhibit SARS-CoV-2 M<sup>Pro</sup> with  $IC_{50}$  values in the micromolar range. In particular, two compounds, cefpiramide sodium and ceftibuten dehydrate, showed an  $IC_{50}$  value around  $30 \mu M$ , while ceforanide, ceftaroline fosamil, and cefaclor inhibited SARS-CoV-2 M<sup>Pro</sup> within a range of 14.9–24  $\mu M$  (Table 2). Moreover, cefadroxil and cefoperazone blocked

**Table 2. Inhibition of SARS-CoV-2 M<sup>Pro</sup> Activity by Compounds**

compound	SARS-CoV-2 M <sup>Pro</sup> $IC_{50}$ ( $\mu M$ )
betrixaban	$0.9 \pm 0.0053$
cefaclor	$24.0 \pm 5.65$
cefadroxil	$2.4 \pm 0.1$
cefoperazone	$4.9 \pm 0.6$
ceforanide	$14.9 \pm 4.1$
cefpiramide sodium	$30.0 \pm 0.1$
ceftaroline fosamil	$18.7 \pm 5.3$
ceftibuten dihydrate	$30.0 \pm 0.1$
diosmin	>30 (68%)
isavuconazole	>30 (57%)
NADH	>30 (55%)
PF-03715455	>30 (100%)
PF-00610355	>30 (100%)
polydatin	>30 (66%)
reproterol	>30 (100%)
rutin	>30 (100%)
zafirlukast	>30 (100%)
GC376	$0.00014 \pm 0.00001$

<sup>a</sup>Compound concentration required to reduce enzyme activity by 50%.

the M<sup>Pro</sup> protease activity with  $IC_{50}$  values in the low micromolar range (2.4–4.9  $\mu M$ ). It is worth noting that betrixaban was able to hamper *in vitro* the enzymatic activity of M<sup>Pro</sup> with submicromolar  $IC_{50}$  values (Table 2).

Analyzing the *in vitro* enzymatic assays' results, it was noted that the most interesting compounds belong to the class of cephalosporin drugs and oral anticoagulants.

Cephalosporins are  $\beta$ -lactams widely used antibacterial drugs, but it was demonstrated that they could also inhibit other classes of nucleophilic enzymes, such as human cathepsins, viral cysteine proteases, and mycobacterial L,D-transpeptidases.<sup>33–37</sup> Recently, Malla and co-workers obtained

some penicillin derivatives as potent M<sup>Pro</sup> inhibitors and, by using mass spectrometric and crystallographic analyses, they elucidated their mechanism, which involves a reaction with the nucleophilic cysteine to form a stable acyl-enzyme.<sup>37</sup> All these data promote the study of  $\beta$ -lactams, in particular cephalosporin drugs, for other therapeutics indications, including the treatment of COVID-19 and other viral diseases.

Betrixaban competitively and directly inhibits the serine-protease factor Xa, thus preventing the conversion from prothrombin to thrombin and, in turn, disrupting the coagulation cascade.<sup>38,39</sup> Additionally, along other inhibitors of the Xa factor, such as apixaban and rivaroxaban, betrixaban has been studied for the potential antiviral activity against coronaviruses including SARS-CoV-2,<sup>40,41</sup> thus enforcing our findings.

**Binding Mode Analysis of the Active Compounds Complexed to M<sup>Pro</sup>.** By analyzing the binding modes of the best candidates, betrixaban, cefaclor, cefadroxil, cefoperazone, ceforanide, cefpiramide sodium, ceftaroline fosamil, and ceftibuten dihydrate complexed to the most representative receptor structure of SARS-CoV-2 M<sup>Pro</sup>, we observed that all compounds engaged in favorable interactions with the three substrate-binding subsites (S1, S2, and S4) of the enzyme.

Specifically, as reported in Figure 1A, betrixaban was involved in 3 crucial hydrogen bonds (HBs) with Gly143, Ser144, and the catalytic Cys145. The ligand was further stabilized through a  $\pi$ - $\pi$  stacking interaction with His41 and an HB and a salt-bridge with Glu166, which is essential for keeping the S1 pocket in the correct shape and the enzyme in the active conformation.<sup>6</sup> Concerning cefaclor binding mode, the oxygen of its  $\beta$ -lactam ring was bound to histidine at position 41, also involved in a  $\pi$ - $\pi$  stacking interaction with the phenyl ring of the drug (Figure 1B), while cefadroxil and cefoperazone, two broad-spectrum antibiotic agents used in the treatment of respiratory tract infections, peritonitis, skin infections, endometritis, and bacterial septicemia,<sup>42</sup> were found to establish pivotal HBs with Cys145 and Glu166. Moreover, the phenol OH group of both cefadroxil and cefoperazone was involved in 2 HBs with Thr190 and Gln192. Cefoperazone was further stabilized by means of a  $\pi$ - $\pi$  stacking interaction between its tetrazole ring and histidine at position 41, while cefadroxil was found to engage an additional HB with Ser144 (Figure 1C,D). As reported in Figure 1E, ceforanide, a semisynthetic second-generation cephalosporin, was involved in HBs with Thr26, His41, Cys145, Glu166, and Gln192, while cefpiramide sodium, a third-generation cephalosporin antibiotic, active against *Pseudomonas aeruginosa* and characterized by a broad spectrum of antibacterial activity, was involved in several HBs with Cys145, Glu166, and Thr190. The compound was further stabilized by a  $\pi$ - $\pi$  stacking interaction between its tetrazole ring and His41 (Figure 1F). Ceftaroline fosamil, an advanced-generation parental cephalosporin used to treat community-acquired bacterial pneumonia,<sup>43</sup> made 4 HB interactions with Thr25, Ser46, Gly143, and Glu166 (Figure 1G), while the third-generation cephalosporin ceftibuten, commonly used in the treatment of acute bacterial exacerbations of chronic bronchitis, acute bacterial otitis media, pharyngitis, and tonsillitis was engaged in an HB with Gly143 and a  $\pi$ - $\pi$  stacking interaction with His41 (Figure 1H). All the analyzed drugs were also involved in several hydrophobic contacts with Leu27, Val42, Met49, Met165, Leu167, and Pro168 residues, thus enhancing their binding to the active site of SARS-CoV-2 M<sup>Pro</sup>.

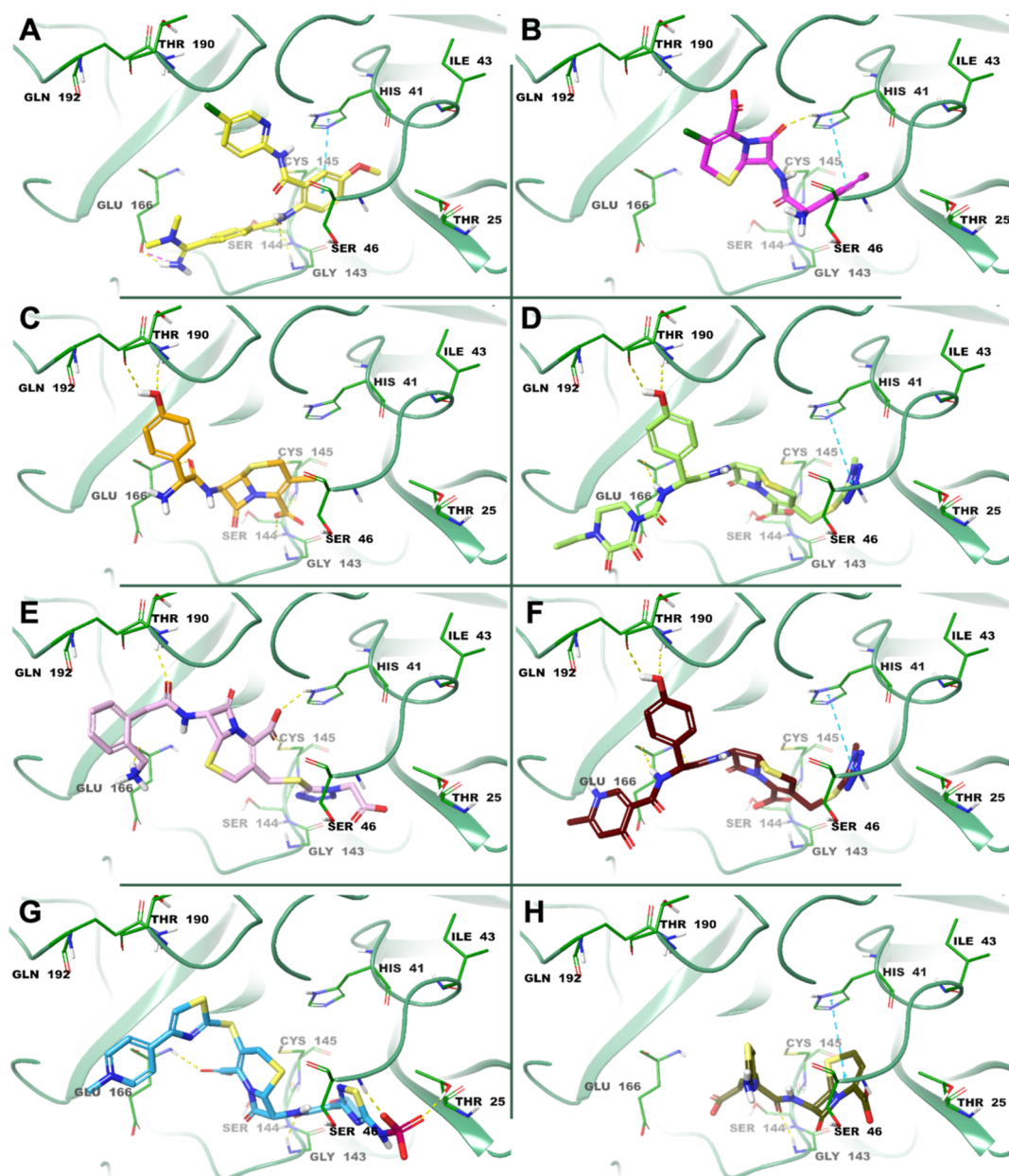


**Figure 1.** 3D representation of the binding modes of (A) betrixaban (yellow), (B) cefaclor (magenta), (C) cefadroxil (light orange), (D) cefoperazone (light green), (E) ceforanide (pink), (F) cefpiramide sodium (burgundy), (G) ceftaroline fosamil (cyan), and (H) ceftibuten (olive) complexed to the most representative receptor structure of SARS-CoV-2  $M^{pro}$ . The protein is shown as forest cartoon, while the drugs are reported as sticks. The HBs, salt-bridge, and stacking interactions are indicated as yellow, magenta, and cyan dashed lines, respectively.

The 2D binding mode of the inactive compounds in complex with SARS-CoV-2  $M^{pro}$  is reported in [Supporting Information](#), Figure S1.

With the aim to study in more detail the binding of the 7 cephalosporins into the active site, we employed a covalent docking strategy. As reported in [Figure 2](#), the carbonyl oxygen of all  $\beta$ -lactams was found to interact with the backbone of Gly143 and Cys145, which represent the oxyanion hole. The sole exception was observed for ceftibuten, in which only two carboxyl moieties were able to bind Ser46, Gly143, and His163. The carboxyl group of cefaclor interacted with Glu166 via one HB, while ceftaroline was stabilized by 4HBs and a salt bridge with Ser1, Thr26, Phe140, and Leu141. Cefpiramide engaged 3 HBs with the backbone atoms of Thr26 and His164, and the side chain of Glu166, while ceforanide interacted with

Thr24, Asn142, and Glu166. Finally,  $M^{pro}$  Asn142, His164, and Glu166 residues were responsible for the stabilization of cefadroxil and cefoperazone, with the last one drug able to establish an additional HB with Thr25.

**Molecular Dynamics Analysis of the Active Compounds Complexed to  $M^{pro}$ .** In order to further investigate the behavior of the ligand- $M^{pro}$  complexes, 200 ns of MDs were performed starting from the docking pose of the 8 best candidates complexed to the most representative receptor structure of SARS-CoV-2  $M^{pro}$ . Desmond software,<sup>44</sup> with the parameters reported in the experimental section, was used for MDs. During the whole trajectory, for each complex, the protein backbone RMSD trend was calculated, and as reported in [Figure 3](#), betrixaban and all the cephalosporin derivatives were found to similarly stabilize the protein structure.

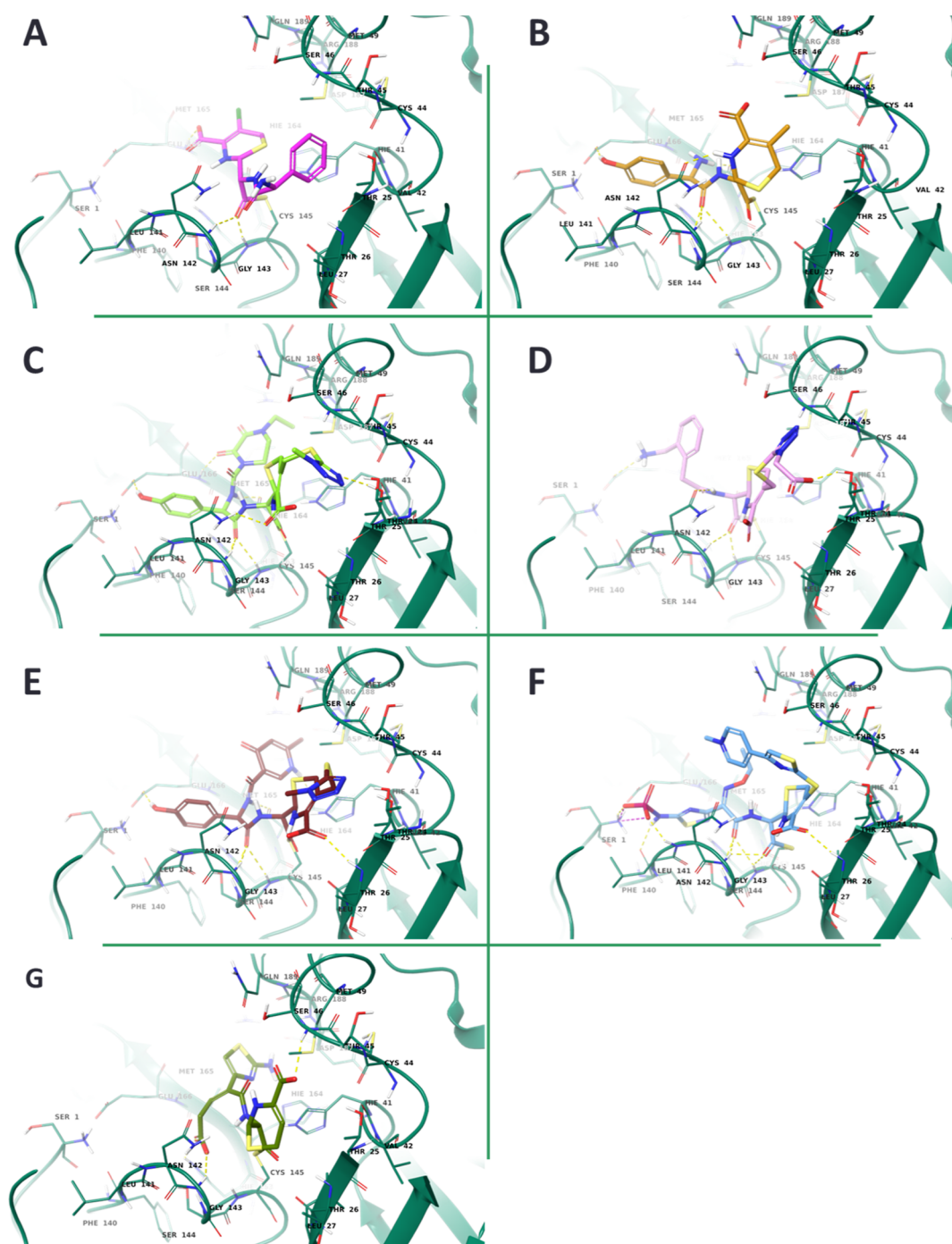


**Figure 2.** 3D representation of the covalent binding modes of (A) cefaclor (magenta), (B) cefadroxil (light orange), (C) cefoperazone (light green), (D) ceforanide (pink), (E) cefpiramide sodium (burgundy), (F) ceftaroline fosamil (cyan), and (G) cefibuten (olive) to SARS-CoV-2 M<sup>Pro</sup> catalytic site. The protein is shown as forest cartoon, while the drugs are reported as sticks. The HBs and salt-bridge are indicated as yellow and magenta dashed lines, respectively.

Moreover, for each ligand, we calculated the root mean square fluctuation (RMSF), in order to evaluate the ligand atom position changes during the whole simulation and the fluctuations of each ligand within the complex (Figure 4).

The general pattern of fluctuation was found to be moderately lower for betrixaban and cefoperazone compared to the other drugs. Specifically, as reported in Figure 5, we observed that, in the second part of the simulation, the distance between the oxygen atom of M<sup>Pro</sup> Glu166 carboxylate and the protonated nitrogen atom of betrixaban carbamimidoyl

group always stayed below 3 Å. The lower RMSF trend of the anticoagulant agent into the M<sup>Pro</sup> binding pocket could be justified by its ability to maintain this pivotal salt-bridge interaction with Glu166 during MDs, thus assuring a remarkable electrostatic contribution in the complex stabilization.

**Conservation Analysis.** In order to identify druggable targets and to investigate antiviral compounds, the conservation analysis and a detailed examination of SARS-CoV-2 M<sup>Pro</sup> residues are essential. In this light, a comprehensive

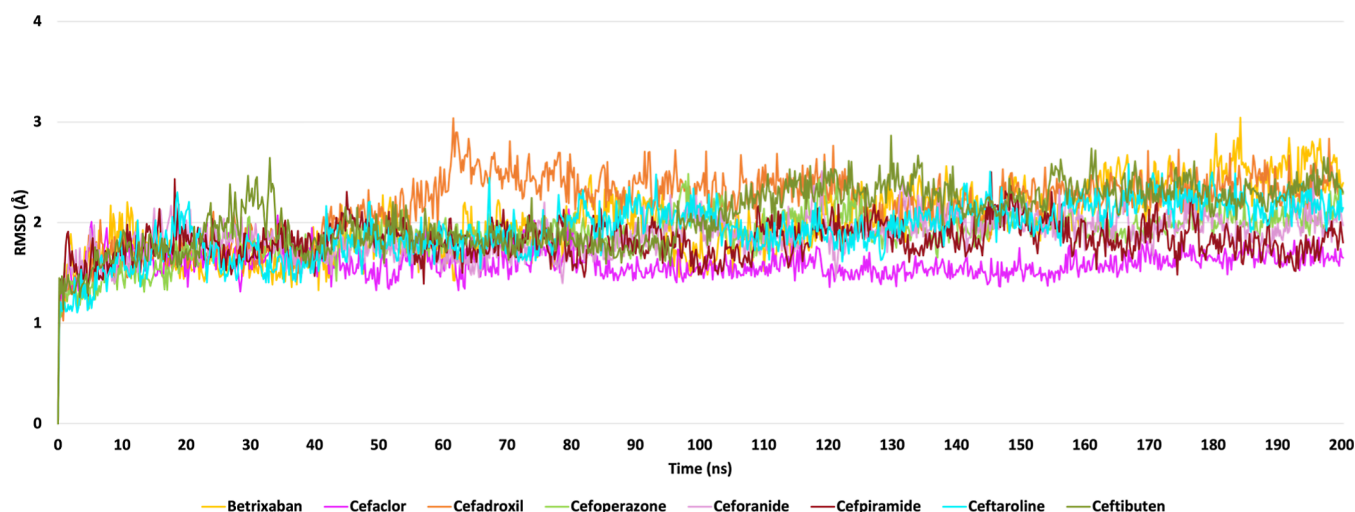


**Figure 3.**  $M^{Pro}$  protein backbone RMSD trend calculated in the presence of betrixaban (yellow line), cefaclor (magenta line), cefadroxil (light orange line), cefoperazone (light green line), ceforanide (pink line), cefpiramide sodium (burgundy line), ceftaroline fosamil (cyan line), and ceftibuten (olive line). The RMSD values are expressed in Å.

analysis of the entire  $M^{Pro}$  was performed by using over 13.7 million SARS-CoV-2 sequences. The analysis revealed an extremely high degree of conservation in the entire  $M^{Pro}$ . Notably, 62.4% (191/306) of residues never mutated, and 36.6% (112/306) were extremely conserved in >99.5% of the sequences analyzed (Figure 6). Among the remaining three residues, two (at residues 89 and 90) showed a substantial degree of conservation >98.5% (Figure 6), with the mutations Leu89Phe and Lys90Arg being detected exclusively in the early variants as Beta and Delta.

Only one residue at position 132 was found to be frequently mutated in 47.5% of the sequences, mainly due to the occurrence of Pro132His, which characterizes the backbone of Omicron variants including the currently circulating subvariants, BQ.x, and BF.x. Conversely, this mutation has never been detected in any of the previously circulating variants. Importantly, it is noteworthy to mention that Pro132His lies in a region between the catalytic (at positions 44 and 145) and the dimerization domains (at positions 301–306)<sup>45</sup> and is not responsible for any direct structural changes to the active site. In early 2022, during the surge of the Omicron variant, a study showed that Pro132His led to decrease thermal stability of  $M^{Pro}$  without compromising its catalytic activity or small-molecule drug inhibition.<sup>46</sup> Of note, the residue 166, which has been associated with Paxlovid resistance,<sup>47</sup> was extremely conserved in >99.9% of the analyzed sequences with mutations detected in about 5200 sequences (mostly Glu166Gln). More importantly, focusing our conservation analysis on the 50 residues localized in domains that are crucial for the efficient binding of the tested compounds (aa: 19–28; 39–49; 117–120; 140–145; 163–172; 181 and 186–193), we found that 60% (30/50) of these residues never mutated, while 40% (20/50) were extremely conserved in >99.5%. These data again support the extreme degree of conservation of the  $M^{Pro}$ , particularly in those domains crucial for its enzymatic activity and that are targeted by the antiviral compounds emerged in this study, thus reinforcing the role of  $M^{Pro}$  as an attractive target for antiviral drugs, with broad spectrum activity against all SARS CoV-2 variants.

**SARS-CoV-2 Replication Assay of the Candidate Drugs.** The ability of the most promising compounds in

affecting SARS-CoV-2 replication has been assessed *in vitro* against the replication of SARS-CoV-2 in cell-based assays at 30  $\mu$ M. Among the 17 investigated compounds, betrixaban was able to significantly reduce the viral-induced cytopathic effect showing an  $EC_{50}$  of  $28.5 \pm 2 \mu$ M and no cytotoxicity at the highest concentration tested (Table 3).

COVID-19 induces thrombotic and thromboembolic events in infected patients, caused by excessive inflammation, endothelial cell activation and injury, platelet activation, and hypercoagulability.<sup>48</sup> Independently of age, this complex scenario, known as COVID-19-associated coagulopathy (CoAC), is due to the thrombin generation and fibrinolysis shutdown, representing the causative factors in establishing the environment for pulmonary micro and macrovascular thrombosis and negative consequences. Indeed, CoAC increases morbidity and mortality, especially in patients with acute respiratory distress syndrome.<sup>49</sup>

Our outcomes highlighted that betrixaban is able to block the SARS-CoV-2 replication, and this result is of particular interest since betrixaban has been approved for thromboprophylaxis in hospitalized medically ill patients for its ability to significantly reduce asymptomatic and symptomatic venous thromboembolism (VTE) and VTE-related deaths.<sup>50</sup> In addition, betrixaban is characterized by an important anticoagulant effect over 24 h, no contraindication in patients with severe renal insufficiency and a low propensity for drug–drug interactions.<sup>51</sup>

In line with these findings, betrixaban could be a good therapeutic option for thromboprophylaxis in hospitalized COVID-19 patients.<sup>52</sup>

## CONCLUSIONS

Here, we have presented a successful example of *in silico* drug repurposing approach, which led to the identification of 8 promising  $M^{Pro}$  inhibitors among the FDA-approved and investigational drugs. Indeed, among the 17 predicted best *hits*, 7 cephalosporins inhibited the  $M^{Pro}$  activity in the micromolar range (with 47% of success) and the most potent compound, the oral anticoagulant betrixaban, was also able to inhibit the viral replication in the sub-micromolar range.

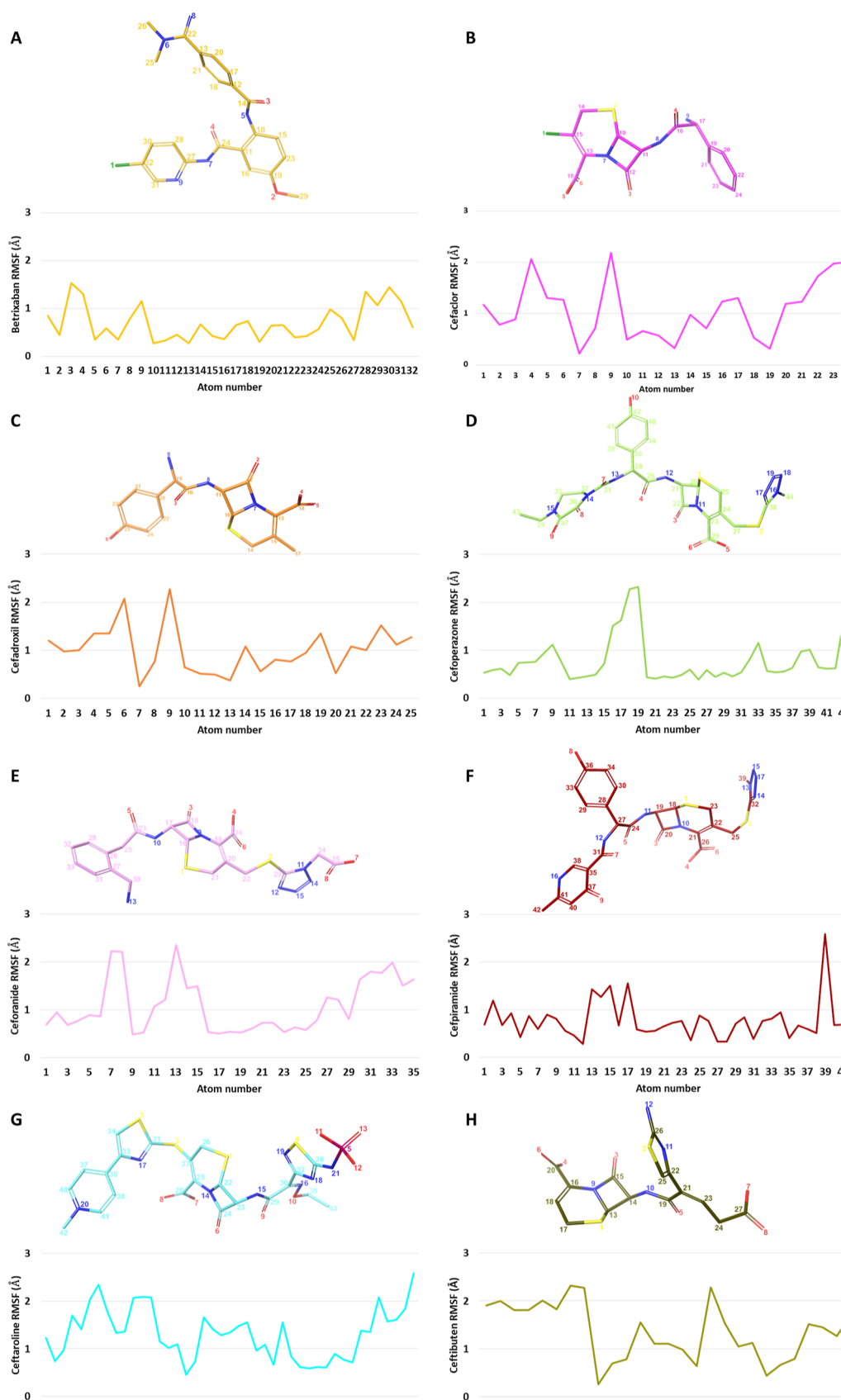


**Figure 4.** RMSF plots of (A) betrixaban (yellow line), (B) cefaclor (magenta line), (C) cefadroxil (light orange line), (D) cefoperazone (light green line), (E) ceforanide (pink line), (F) ceftipamide sodium (burgundy line), (G) ceftaroline fosamil (cyan line), and (H) ceftibuten (olive line). The RMSF values expressed in Å and the ligand atom number are reported on the ordinate and abscissa axes, respectively.

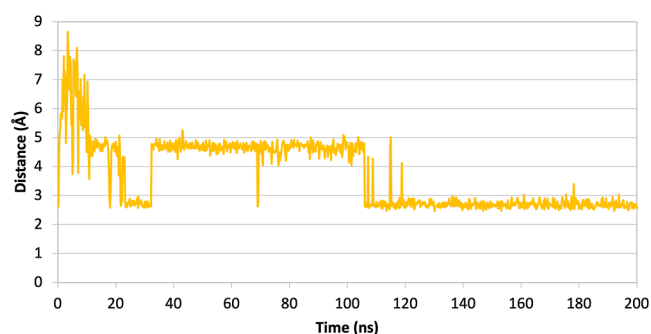


**Figure 5.** Monitoring of the distance between the oxygen atom of  $M^{\text{Pro}}$  Glu166 carboxylate and the protonated nitrogen atom of betrixaban carbamimidoyl group during the whole MDs. The distance is expressed in Å.

Due to its high degree of conservation, emerged from our analysis of >13 million SARS-CoV-2 sequences,  $M^{\text{Pro}}$  could be considered as a suitable target for antiviral therapy aiming to thwart the genetic evolution that SARS-CoV-2 is undergoing. In particular, we also proved the high extent of conservation (>99.5%) of the protease residues deemed important to the enzymatic activity, pivotal for the binding of the antiviral compounds identified in this study, thus emphasizing their potential to guarantee a wide-spectrum effectiveness against all SARS-CoV-2 variants. Recent evidence has also confirmed previous data indicating that the  $M^{\text{Pro}}$  exhibits a significant degree of conservation across the entire coronavirus family, supporting its role as target for compounds endowed of robust pancoronavirus antiviral activity,<sup>53</sup> thus critical in facing the emergence of novel coronaviruses.

Interestingly, the effect of betrixaban in affecting SARS-CoV-2 replication could be combined with its already known feature

**Table 3.** Viral Replication Assays

compound	SARS-CoV-2 $EC_{50}$ ( $\mu\text{M}$ ) <sup>a</sup>	VEROE6-GFP $CC_{50}$ ( $\mu\text{M}$ ) <sup>b</sup>	SI
betrixaban	28.5 ± 2.3	>100 (92%) <sup>d</sup>	>3.5
cefaclor	>30 (92%) <sup>c</sup>	>30 (92%)	ND
cefadroxil	>30 (108%)	>30 (85%)	ND
cefoperazone	>30 (92%)	>30 (97%)	ND
ceforanide	>30 (100%)	>30 (104%)	ND
cefpiramide sodium	>30 (94%)	>30 (95%)	ND
ceftaroline fosamil	>30 (105%)	>30 (105%)	ND
ceftibuten dihydrate	>30 (95%)	>30 (96%)	ND
diosmin	>30 (103%)	44%	ND
isavuconazole	>30 (92%)	>30 (94%)	ND
NADH	>30 (97%)	>30 (93%)	ND
PF-03715455	>30 (100%)	>30 (86%)	ND
PF-00610355	>30 (99%)	>30 (104%)	ND
polydatin	>30 (106%)	>30 (88%)	ND
reproterol	>30 (89%)	>30 (100%)	ND
rutin	>30 (92%)	>30 (99%)	ND
zafirlukast	>30 (90%)	>30 (92%)	ND
GC376	0.4 ± 0.2	>100 (100%)	>250

<sup>a</sup> $EC_{50}$  = concentration of compound that gives 50% rescue of the virus-reduced eGFP signals as compared to the untreated virus-infected control cells. <sup>b</sup> $CC_{50}$  = 50% cytotoxic concentration, as determined by measuring the cell viability. <sup>c</sup>Percentage of residual CPE at the highest concentration tested. <sup>d</sup>Percentage of residual cellular viability at the highest concentration tested. The values represent the means ± SD of data derived from duplicate experiments. SI = selectivity index calculated as the ratio between  $CC_{50}$  and  $EC_{50}$  of each compound.

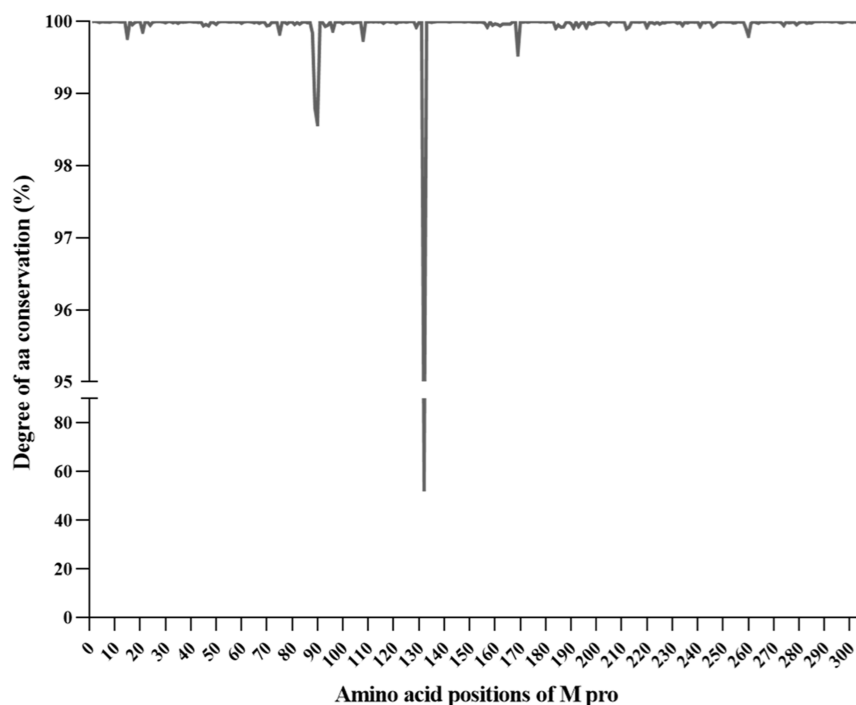


**Figure 6.** Genomic plot reporting the genetic conservation of SARS-CoV-2  $M^{\text{Pro}}$ . Dotted line represents the cut-off of amino acid conservation (99.5%) used to define highly conserved residues. The only three amino acid positions characterized by a conservation <99.5% are reported in the graph.



on preventing VTE, giving a positive contribution to the outcome of COVID-19 patients. Thus, considering its ability to reduce SARS-CoV-2 viral load and to prevent the thrombotic and thromboembolic events, our results could pave the way for a possible use of betrixaban in the treatment of hospitalized COVID-19 patients.

In conclusion, our *in silico* and *in vitro* data may provide information to drive medicinal chemistry projects to find more promising derivatives and/or evaluate the combination with other anti-SARS-CoV-2 drugs to potentiate their effects with respect to their original benefits.

## EXPERIMENTAL SECTION

**Molecular Modeling.** Starting from the crystal structure of the complex resulting from the reaction between SARS-CoV-2 main protease and *tert*-butyl (1-((*S*)-1-(((*S*)-4-(benzylamino)-3,4-dioxo-1-((*S*)-2-oxopyrrolidin-3-yl)butan-2-yl)amino)-3-cyclopropyl-1-oxopropan-2-yl)-2-oxo-1,2-dihydropyridin-3-yl)-carbamate (alpha-ketoamide 13b), deposited in the PDB with the PDB code 6Y2G,<sup>6</sup> our molecular modeling studies were carried out. To assess the accuracy and reliability of our docking protocol, first we performed re-docking calculations of the co-crystallized ligand by using Glide software v.6.7, with the standard precision (SP) algorithm, generating 10 poses per ligand.<sup>54</sup> In order to evaluate the geometrical reproduction of the experimental data, the RMSD between the X-ray and the ligand best docking pose was analyzed (RMSD value equal to 1.665 Å).

The receptor structure was properly processed using the Protein Preparation Wizard tool.<sup>55</sup> Hydrogens were added and disulfide bonds were created. Missing side chains and missing loops were added using Prime. The hydrogen bonding network was optimized and the  $pK_a$  values of the residues along with their protonation state were calculated at pH 7.4.<sup>55</sup> The complex was then submitted to 10,000 MacroModel energy minimization steps, using OPLS\_2005 as force field.<sup>56</sup>

In order to explore all the conformational states of the complex, 200 ns of MDs were carried out. The MDs were run using Desmond package v5.3. The system was immersed in an orthorhombic box of TIP4P water molecules, extending at least 10 Å from the protein and counter ions were added to neutralize the system charge. The system temperature was set at 300 K and the *NPT* ensemble was selected.<sup>44</sup> The resulting trajectory was clustered with respect to the RMSD in order to explore the collection of all the obtained structures, getting 4 representative structures, which were submitted to 10,000 MacroModel energy minimization steps, using OPLS-2005 as force field.<sup>56</sup> All the obtained conformations were used for further molecular recognition studies, carried out with Glide software v.7.8, by using the SP algorithm and by generating 10 poses per ligand.<sup>54</sup> The consensus docking score (*D*-score) was calculated for both energy minimized and unminimized structures. By comparing the obtained average values (*D*-score<sub>av-min</sub> = -7.10 kcal/mol and *D*-score<sub>av-not min</sub> = -9.50 kcal/mol), the best theoretical binding affinity was observed for the unminimized structures. After virtual screening studies, the obtained compounds were ranked according to their *D*-score value and, starting from the best theoretical binding affinity score, 200 compounds were selected. By means of a visual inspection and based on their commercial availability, 17 best *hits* were purchased and submitted to biological evaluations. Finally, the cephalosporins were selected for covalent docking. Each ligand was covalently docked at Cys145 using a box size

≤20 Å, employing the reaction “β-lactam addition” and the SMARTS “[O-0X1] = [C]1[C][C][N]1” for recognition of reacting groups. Docking was performed in the “Pose Prediction (Thorough)” mode, employing a cutoff of 2.5 kcal mol<sup>-1</sup> to retain poses for further refinement, and a maximum of 100 poses for refinement. Scoring was calculated using Glide and one pose was out-put per reaction site.

The best docking pose of the 8 selected compounds was submitted to 200 ns MDs. The MDs were carried out by applying the same protocol described above. The Simulation Interaction Diagram tool implemented in Desmond v. 3.8<sup>44</sup> was used to analyze the behavior of the ligands and the protein. The analysis included also the RMSD and RMSF calculations evaluated during the whole simulation.

For the virtual screening studies, we used a library of 8791 small molecules (approved drugs, experimental and investigational compounds, and nutraceuticals) obtained from the DrugBank database.<sup>57</sup> The library was prepared using the LigPrep tool.<sup>58</sup> Hydrogens were added, salts were removed, and ionization states were calculated using Epik at pH 7.4. Each structure was submitted to 10,000 MacroModel minimization steps using the OPLS\_2005 as force field.<sup>56,59</sup>

**Pan Assay Interference Compounds Evaluation.** The pan assay interference compounds (PAINS) properties of the 8 active compounds were theoretically investigated by means of the ZINC PAINS Pattern Identifier web server.<sup>60</sup> The method did not highlight any PAINS related to the investigated molecules.

**SARS-CoV-2 M<sup>Pto</sup> Expression and Purification.** SARS-CoV-2 M<sup>Pto</sup> was expressed and transformed in *Escherichia coli* BL21 (DE3) cells, as described in Pelliccia et al. in 2022.<sup>61,62</sup> The protein was purified using a two-step process. The purified protein fractions were pooled and subjected to buffer exchange (20 mM Tris-HCl, 150 mM NaCl, 1 mM EDTA, 1 mM DTT, and pH 7.8) by using Amicon Ultra 15 centrifugal filters at 4000×g, at 4 °C, aliquoted and stored at -80 °C. The protein purity was checked by SDS-PAGE analysis.

**Determination of SARS-CoV-2 M<sup>Pto</sup> Activity.** Enzymatic activity and inhibition of SARS-CoV-2 M<sup>Pto</sup> was assessed using a FRET assay, as described in Kuzikow et al.<sup>56,64</sup> Briefly, SARS-CoV-2 M<sup>Pto</sup> was pre-incubated with different concentrations of the compounds at 37 °C for 30 min, in a reaction mix containing 20 mM Tris-HCl pH 7.3, 100 mM NaCl, and 1 mM EDTA. Subsequently, 12 μM of FRET substrate (peptide DABCYL-KTSAVLQ↓SGFRKM-EDANS) was added and the reaction was conducted at room temperature for 15 min, after which the fluorescent signal (ex/em 320/480) was acquired.

**Conservation Analysis.** The SARS-CoV-2 genome sequences (*N* = 13,729,050) were retrieved until 12 Dec 2022 from the GISAID database and used to accurately define any amino acid substitution in the main protease (M<sup>Pto</sup>) of SARS-CoV-2 (amino acid 1–306). By applying a stringent quality filter, only entire sequences with high quality were included in this study. High-quality sequences were defined as genomes of >29,000 nucleotides, characterized by the presence of <5% ambiguous nucleotides and <0.05% unique amino acid mutations. The Bioedit software and MAFFT server were used to align sequences against the reference sequence (NC\_045512.2 SARS-CoV-2-Wuhan-Hu-1 isolate). Then, the alignments were split into different proteins to set apart M<sup>Pto</sup> sequences. Sequences with a mixture of wild-type and mutant residues at single positions were considered to have the mutant(s) at that position. Finally, based on alignment

conservation annotation, we measured the overall degree of M<sup>Pro</sup> conservation by measuring the number of conserved amino acids for each column (position) of the alignment. To standardize the effect of the sequence, the prevalence of mutations at each amino acid positions was calculated based on total representative sequences while considering the sample size and margin of error; a 99.5% confidence interval was, thus, set as the limit for defining highly conserved positions.

**SARS-CoV-2 Replication Assay.** SARS-CoV-2 replication assay was performed according to the protocol reported by Corona et al. in 2021.<sup>63</sup> African green monkey kidney-engineered cells were used to constitutively express GFP (Vero E6-GFP) provided by Janssen Pharmaceutical. SARS-CoV-2 strain BetaCov/Belgium/GHB-03021/2020 was provided by KU Leuven. GC376 compound<sup>64</sup> was used as positive control, in presence of 2 mM p-gp inhibitor CP-100356.<sup>65</sup> Assay was read at 72 h post infection.

**Evaluation of Cytotoxicity.** The assay was performed according to the protocol reported by Corona et al. in 2022<sup>63</sup> using Vero E6-GFP cells. Results were checked at 72 h post infection.

## ■ ASSOCIATED CONTENT

### SI Supporting Information

The Supporting Information is available free of charge at <https://pubs.acs.org/doi/10.1021/acs.jcim.3c00282>.

Molecular modeling analysis: Table S1. Molecular formula strings of selected compounds. Figure S1: 2D representation of (A) diosmin; (B) isavuconazole; (C) NADH; (D) PF-00610355; (E) PF-03715455; (F) polydatin; (G) reprotoleol; (H) rutin; and (J) zafirlukast in complex with SARS-CoV-2 M<sup>Pro</sup>. PDB structure of M<sup>Pro</sup>. PDB complex of betrixaban in complex with M<sup>Pro</sup>. PDB complex of cefaclor in complex with M<sup>Pro</sup>. PDB complex of cefradroxil in complex with M<sup>Pro</sup>. PDB complex of cefoperazone in complex with M<sup>Pro</sup>. PDB complex of ceforanide in complex with M<sup>Pro</sup>. PDB complex of cefpiramide in complex with M<sup>Pro</sup>. PDB complex of ceftaroline in complex with M<sup>Pro</sup>. PDB complex of ceftibuten in complex with M<sup>Pro</sup> (PDF)

## ■ AUTHOR INFORMATION

### Corresponding Author

**Giosuè Costa** – Dipartimento di Scienze della Salute and Net4Science Academic Spin-Off, Università degli Studi “Magna Græcia” di Catanzaro, 88100 Catanzaro, Italy; [orcid.org/0000-0003-0947-9479](https://orcid.org/0000-0003-0947-9479); Email: [gcosta@unicz.it](mailto:gcosta@unicz.it)

### Authors

**Francesca Alessandra Ambrosio** – Dipartimento di Medicina Sperimentale e Clinica, Università degli Studi “Magna Græcia” di Catanzaro, 88100 Catanzaro, Italy; [orcid.org/0000-0003-4874-2946](https://orcid.org/0000-0003-4874-2946)

**Isabella Romeo** – Dipartimento di Scienze della Salute and Net4Science Academic Spin-Off, Università degli Studi “Magna Græcia” di Catanzaro, 88100 Catanzaro, Italy; [orcid.org/0000-0002-5799-7863](https://orcid.org/0000-0002-5799-7863)

**Francesca Esposito** – Department of Life and Environmental Sciences, University of Cagliari, Cittadella Universitaria di Monserrato, 09124 Cagliari, Italy

**Mohammad Alkhatib** – Dipartimento di Medicina Sperimentale, Università degli Studi di Roma “Tor Vergata”, 00133 Roma, Italy

**Romina Salpini** – Dipartimento di Medicina Sperimentale, Università degli Studi di Roma “Tor Vergata”, 00133 Roma, Italy

**Valentina Svicher** – Dipartimento di Medicina Sperimentale, Università degli Studi di Roma “Tor Vergata”, 00133 Roma, Italy

**Angela Corona** – Department of Life and Environmental Sciences, University of Cagliari, Cittadella Universitaria di Monserrato, 09124 Cagliari, Italy; [orcid.org/0000-0002-6630-8636](https://orcid.org/0000-0002-6630-8636)

**Paolo Malune** – Department of Life and Environmental Sciences, University of Cagliari, Cittadella Universitaria di Monserrato, 09124 Cagliari, Italy

**Enzo Tramontano** – Department of Life and Environmental Sciences, University of Cagliari, Cittadella Universitaria di Monserrato, 09124 Cagliari, Italy; [orcid.org/0000-0002-4849-0980](https://orcid.org/0000-0002-4849-0980)

**Francesca Ceccherini-Silberstein** – Dipartimento di Medicina Sperimentale, Università degli Studi di Roma “Tor Vergata”, 00133 Roma, Italy

**Stefano Alcaro** – Dipartimento di Scienze della Salute and Net4Science Academic Spin-Off, Università degli Studi “Magna Græcia” di Catanzaro, 88100 Catanzaro, Italy; [orcid.org/0000-0002-0437-358X](https://orcid.org/0000-0002-0437-358X)

**Anna Artese** – Dipartimento di Scienze della Salute and Net4Science Academic Spin-Off, Università degli Studi “Magna Græcia” di Catanzaro, 88100 Catanzaro, Italy

Complete contact information is available at: <https://pubs.acs.org/doi/10.1021/acs.jcim.3c00282>

### Author Contributions

Conception: F.A.A., G.C., A.A., and S.A. Development of methodology: F.A.A., G.C., F.E., A.C., and R.S. Molecular modeling studies: F.A.A. and G.C. Acquisition of data: F.A.A., G.C., and A.A. Conservation analysis: R.S., M.A., V.S., and F.C.-S. Analysis and interpretation of data: F.A.A., G.C., and A.A. *In vitro* assays: F.E., A.C., and P.M. Drafted the manuscript: F.A.A., A.A., I.R., and F.E. Study supervision: S.A., E.T., and F.C.-S. All authors have given approval to the final version of the manuscript.

### Funding

This work was financially supported by the Piattaforma NoCovid@UMG Progetto POR Calabria-FESR/FSE 2014-2020- Azione 10.5.12 (DDRC no. 4584 del 4/5/2021).

### Notes

The authors declare no competing financial interest. The library used for the virtual screening studies was downloaded from the DrugBank database (<https://go.drugbank.com>). The 2D structure, compound names, and theoretical binding affinity values of the best compounds are provided in the manuscript. The molecular modeling strings of the active compounds are provided in the Supporting Information. The name, average *D*-score, smile, and ICS0 value ( $\mu\text{M}$ ) of the active compounds are reported in an additional file (smiles.txt). All the ligands were prepared by means of the LigPrep tool (Schrödinger suite) using Epik-v4.3 at pH 7.4 and submitted to 10,000 MacroModel-v11.9 minimization steps using OPLS\_2005 as force field (Schrödinger suite). Schrödinger Suite 2018-1 (<https://www.schrodinger.com>)

schrodinger.com) is distributed under license. The crystal structure of the complex resulting from the reaction between SARS-CoV-2 main protease and *tert*-butyl (1-((*S*)-1-(((*S*)-4-(benzylamino)-3,4-dioxo-1-((*S*)-2-oxopyrrolidin-3-yl)butan-2-yl)amino)-3-cyclopropyl-1-oxopropan-2-yl)-2-oxo-1,2-dihydropyridin-3-yl)carbamate (alpha-ketoamide 13b) was retrieved from the PDB (PDB ID: 6Y2G). Hydrogen atoms were added, and disulfide bonds were created. Missing side chains and missing loops were added using Prime. The hydrogen bonding network was optimized and the  $pK_a$  values of the residues along with their protonation state were calculated at pH 7.4 by using Protein Preparation Wizard tool (Schrödinger suite). The complex was then submitted to 10,000 MacroModel-v.11.9 energy minimization steps, using OPLS\_2005 as force field (Schrödinger suite). The MDs were carried out using Desmond package v5.3. (Schrödinger suite). The docking studies were carried out by means of Glide-v.7.8 by using the SP (Schrödinger suite). The PAINS evaluation was performed on the 8 active compounds by means of the ZINC PAINS Pattern Identifier web server (zinc15.docking.org/patterns/home).

## ACKNOWLEDGMENTS

The authors would like to thank Pfizer Inc. for kindly providing experimental compounds PF-03715455 and PF-00610355.

## ABBREVIATIONS

SARS-CoV-2, severe acute respiratory syndrome coronavirus 2; COVID-19, coronavirus disease 2019; (SARS-CoV), acute respiratory syndrome coronavirus; (MERS-CoV), Middle East respiratory syndrome coronavirus; ( $M^{pro}$ ), main protease; 3CL $^{pro}$ , 3-chymotrypsin-like protease; (PL $^{pro}$ ), papain-like protease; RdRp, RNA-dependent RNA polymerase; (pp1a), polyprotein 1a; (pp1ab), 1ab; (HTS), high-throughput screening; FDA, Food and Drug Administration; (NADH), nicotinamide adenine dinucleotide; (HB), hydrogen bond; (PDB), Protein Data Bank; (IC $_{50}$ ), half maximal inhibitory concentration; (MDs), molecular dynamics simulations; (RMSD), root mean square deviation; (SP), standard precision; (*D*-score), docking score; (S1, S2 and S4), substrate-binding subsites; (HBs), hydrogen bonds; (RMSF), root mean square fluctuation; VTE, venous thromboembolism

## REFERENCES

- (1) WHO COVID-19 Dashboard. World Health Organization: Geneva, 2020. Available online. <https://covid19.who.int/> (accessed September 15, 2022).
- (2) Pal, M.; Berhanu, G.; Desalegn, C.; Kandi, V. Severe Acute Respiratory Syndrome Coronavirus-2 (SARS-CoV-2): An Update. *Cureus* **2020**, *12*, No. e7423.
- (3) Fehr, A. R.; Perlman, S. Coronaviruses: an overview of their replication and pathogenesis. *Methods Mol. Biol.* **2015**, *1282*, 1–23.
- (4) Gil, C.; Ginex, T.; Maestro, I.; Nozal, V.; Barrado-Gil, L.; Cuesta-Geijo, M. A.; Urquiza, J.; Ramirez, D.; Alonso, C.; Campillo, N. E.; Martinez, A. COVID-19: Drug Targets and Potential Treatments. *J. Med. Chem.* **2020**, *63*, 12359–12386.
- (5) Jin, Z.; Du, X.; Xu, Y.; Deng, Y.; Liu, M.; Zhao, Y.; Zhang, B.; Li, X.; Zhang, L.; Peng, C.; Duan, Y.; Yu, J.; Wang, L.; Yang, K.; Liu, F.; Jiang, R.; Yang, X.; You, T.; Liu, X.; Yang, X.; Bai, F.; Liu, H.; Liu, X.; Guddat, L. W.; Xu, W.; Xiao, G.; Qin, C.; Shi, Z.; Jiang, H.; Rao, Z.; Yang, H. Structure of  $M^{pro}$  from SARS-CoV-2 and discovery of its inhibitors. *Nature* **2020**, *582*, 289–293.
- (6) Zhang, L.; Lin, D.; Sun, X.; Curth, U.; Drosten, C.; Sauerhering, L.; Becker, S.; Rox, K.; Hilgenfeld, R. Crystal structure of SARS-CoV-

2 main protease provides a basis for design of improved  $\alpha$ -ketoamide inhibitors. *Science* **2020**, *368*, 409–412.

(7) Shi, J.; Wei, Z.; Song, J. Dissection study on the severe acute respiratory syndrome 3C-like protease reveals the critical role of the extra domain in dimerization of the enzyme: defining the extra domain as a new target for design of highly specific protease inhibitors. *J. Biol. Chem.* **2004**, *279*, 24765–24773.

(8) Ullrich, S.; Nitsche, C. The SARS-CoV-2 main protease as drug target. *Bioorg. Med. Chem. Lett.* **2020**, *30*, 127377.

(9) Hu, Q.; Xiong, Y.; Zhu, G. H.; Zhang, Y. N.; Zhang, Y. W.; Huang, P.; Ge, G. B. The SARS-CoV-2 main protease ( $M^{pro}$ ): Structure, function, and emerging therapies for COVID-19. *MedComm* **2022**, *3*, No. e151.

(10) Fu, L.; Ye, F.; Feng, Y.; Yu, F.; Wang, Q.; Wu, Y.; Zhao, C.; Sun, H.; Huang, B.; Niu, P.; Song, H.; Shi, Y.; Li, X.; Tan, W.; Qi, J.; Gao, G. F. Both Boceprevir and GC376 efficaciously inhibit SARS-CoV-2 by targeting its main protease. *Nat. Commun.* **2020**, *11*, 4417.

(11) Dražić, T.; Kühn, N.; Leuthold, M. M.; Behnam, M. A. M.; Klein, C. D. Efficiency Improvements and Discovery of New Substrates for a SARS-CoV-2 Main Protease FRET Assay. *SLAS Discovery* **2021**, *26*, 1189–1199.

(12) Khamto, N.; Utama, K.; Tateing, S.; Sangthong, P.; Rithchumpon, P.; Cheechana, N.; Saiai, A.; Semakul, N.; Punyodom, W.; Meepowpan, P. Discovery of Natural Bisbenzylisoquinoline Analogs from the Library of Thai Traditional Plants as SARS-CoV-2 3CL $^{pro}$  Inhibitors: *In Silico* Molecular Docking, Molecular Dynamics, and *In Vitro* Enzymatic Activity. *J. Chem. Inf. Model.* **2023**, *63*, 2104–2121.

(13) Clyde, A.; Galanie, S.; Kneller, D. W.; Ma, H.; Babuji, Y.; Blaiszik, B.; Brace, A.; Brettin, T.; Chard, K.; Chard, R.; Coates, L.; Foster, I.; Hauner, D.; Kertesz, V.; Kumar, N.; Lee, H.; Li, Z.; Merzky, A.; Schmidt, J. G.; Tan, L.; Titov, M.; Trifan, A.; Turilli, M.; Van Dam, H.; Chennubhotla, S. C.; Jha, S.; Kovalevsky, A.; Ramanathan, A.; Head, M. S.; Stevens, R. High-Throughput Virtual Screening and Validation of a SARS-CoV-2 Main Protease Noncovalent Inhibitor. *J. Chem. Inf. Model.* **2022**, *62*, 116–128.

(14) Gawriljuk, V. O.; Zin, P. P. K.; Puhl, A. C.; Zorn, K. M.; Foil, D. H.; Lane, T. R.; Hurst, B.; Tavella, T. A.; Costa, F. T. M.; Lakshmanane, P.; Bernatchez, J.; Godoy, A. S.; Oliva, G.; Siqueira-Neto, J. L.; Madrid, P. B.; Ekins, S. Machine Learning Models Identify Inhibitors of SARS-CoV-2. *J. Chem. Inf. Model.* **2021**, *61*, 4224–4235.

(15) Njoroge, F. G.; Chen, K. X.; Shih, N. Y.; Piwinski, J. J. Challenges in modern drug discovery: a case study of boceprevir, an HCV protease inhibitor for the treatment of hepatitis C virus infection. *Acc. Chem. Res.* **2008**, *41*, 50–59.

(16) Redhead, M. A.; Owen, C. D.; Brewitz, L.; Collette, A. H.; Lukacik, P.; Strain-Damerell, C.; Robinson, S. W.; Collins, P. M.; Schäfer, P.; Swindells, M.; Radoux, C. J.; Hopkins, I. N.; Fearon, D.; Douangamath, A.; von Delft, F.; Malla, T. R.; Vangeel, L.; Vercruysee, T.; Thibaut, J.; Leyssen, P.; Nguyen, T.; Hull, M.; Tumber, A.; Hallett, D. J.; Schofield, C. J.; Stuart, D. I.; Hopkins, A. L.; Walsh, M. A. Publisher Correction: Bispecific repurposed medicines targeting the viral and immunological arms of COVID-19. *Sci. Rep.* **2021**, *11*, 19633.

(17) Elford, P. R.; Heng, R.; Révész, L.; MacKenzie, A. R. Reduction of inflammation and pyrexia in the rat by oral administration of SDZ 224-015, an inhibitor of the interleukin-1 beta converting enzyme. *Br. J. Pharmacol.* **1995**, *115*, 601–606.

(18) Ma, C.; Sacco, M. D.; Hurst, B.; Townsend, J. A.; Hu, Y.; Szeto, T.; Zhang, X.; Tarbet, B.; Marty, M. T.; Chen, Y.; Wang, J. Boceprevir, GC-376, and calpain inhibitors II, XII inhibit SARS-CoV-2 viral replication by targeting the viral main protease. *Cell Res.* **2020**, *30*, 678–692.

(19) Hoffman, R. L.; Kania, R. S.; Brothers, M. A.; Davies, J. F.; Ferre, R. A.; Gajiwala, K. S.; He, M.; Hogan, R. J.; Kozminski, K.; Li, L. Y.; Lockner, J. W.; Lou, J.; Marra, M. T.; Mitchell, L. J., Jr; Murray, B. W.; Nieman, J. A.; Noell, S.; Planken, S. P.; Rowe, T.; Ryan, K.; Smith, G. J., 3rd; Solowiej, J. E.; Stepan, C. M.; Taggart, B. Discovery of Ketone-Based Covalent Inhibitors of Coronavirus 3CL Proteases

for the Potential Therapeutic Treatment of COVID-19. *J. Med. Chem.* **2020**, *63*, 12725–12747.

(20) Yang, H.; Xie, W.; Xue, X.; Yang, K.; Ma, J.; Liang, W.; Zhao, Q.; Zhou, Z.; Pei, D.; Ziebuhr, J.; Hilgenfeld, R.; Yuen, K. Y.; Wong, L.; Gao, G.; Chen, S.; Chen, Z.; Ma, D.; Bartlam, M.; Rao, Z. Design of wide-spectrum inhibitors targeting coronavirus main proteases. *PLoS Biol.* **2005**, *3*, No. e324.

(21) Pillaiyar, T.; Manickam, M.; Namasivayam, V.; Hayashi, Y.; Jung, S. H. An Overview of Severe Acute Respiratory Syndrome-Coronavirus (SARS-CoV) 3CL Protease Inhibitors: Peptidomimetics and Small Molecule Chemotherapy. *J. Med. Chem.* **2016**, *59*, 6595–6628.

(22) Douangamath, A.; Fearon, D.; Gehrtz, P.; Krojer, T.; Lukacik, P.; Owen, C. D.; Resnick, E.; Strain-Damerell, C.; Aimon, A.; Abrányi-Balogh, P.; Brandão-Neto, J.; Carbery, A.; Davison, G.; Dias, A.; Downes, T. D.; Dunnett, L.; Fairhead, M.; Firth, J. D.; Jones, S. P.; Keeley, A.; Keserü, G. M.; Klein, H. F.; Martin, M. P.; Noble, M. E. M.; O'Brien, P.; Powell, A.; Reddi, R. N.; Skyner, R.; Snee, M.; Waring, M. J.; Wild, C.; London, N.; von Delft, F.; Walsh, M. A. Crystallographic and electrophilic fragment screening of the SARS-CoV-2 main protease. *Nat. Commun.* **2020**, *11*, 5047.

(23) Günther, S.; Reinke, P. Y. A.; Fernández-García, Y.; Lieske, J.; Lane, T. J.; Ginn, H. M.; Koua, F. H. M.; Ehart, C.; Ewert, W.; Oberthuer, D.; Yefanov, O.; Meier, S.; Lorenzen, K.; Krichel, B.; Kopicki, J. D.; Gelisio, L.; Brehm, W.; Dunkel, I.; Seychell, B.; Gieseler, H.; Norton-Baker, B.; Escudero-Pérez, B.; Domaracky, M.; Saouane, S.; Tolstikova, A.; White, T. A.; Hänle, A.; Groessler, M.; Fleckenstein, H.; Trost, F.; Galchenkova, M.; Gevorkov, Y.; Li, C.; Awel, S.; Peck, A.; Barthelmeß, M.; Schlünzen, F.; Lourdu Xavier, P.; Werner, N.; Andaleeb, H.; Ullah, N.; Falke, S.; Srinivasan, V.; França, B. A.; Schwinger, M.; Brognaro, H.; Rogers, C.; Melo, D.; Zaitseva-Doyle, J. J.; Knoska, J.; Peña-Murillo, G. E.; Mashhour, A. R.; Hennicke, V.; Fischer, P.; Hakanpää, J.; Meyer, J.; Gribbon, P.; Ellinger, B.; Kuzikov, M.; Wolf, M.; Beccari, A. R.; Bourenkov, G.; von Stetten, D.; Pompidor, G.; Bento, I.; Panneerselvam, S.; Karpics, I.; Schneider, T. R.; Garcia-Alai, M. M.; Niebling, S.; Günther, C.; Schmidt, C.; Schubert, R.; Han, H.; Boger, J.; Monteiro, D. C. F.; Zhang, L.; Sun, X.; Pletzer-Zelgert, J.; Wollenhaupt, J.; Feiler, C. G.; Weiss, M. S.; Schulz, E.; Mehrabi, P.; Karničar, K.; Usenik, A.; Loboda, J.; Tidow, H.; Chari, A.; Hilgenfeld, R.; Utrecht, C.; Cox, R.; Zaliani, A.; Beck, T.; Rarey, M.; Günther, S.; Turk, D.; Hinrichs, W.; Chapman, H. N.; Pearson, A. R.; Betzel, C.; Meents, A. X-ray screening identifies active site and allosteric inhibitors of SARS-CoV-2 main protease. *Science* **2021**, *372*, 642–646.

(24) Hammond, J.; Leister-Tebbe, H.; Gardner, A.; Abreu, P.; Bao, W.; Wisemandle, W.; Baniecki, M.; Hendrick, V. M.; Damle, B.; Simón-Campos, A.; Pypstra, R.; Rusnak, J. M. Oral Nirmatrelvir for High-Risk, Nonhospitalized Adults with Covid-19. *N. Engl. J. Med.* **2022**, *386*, 1397–1408.

(25) Owen, D. R.; Allerton, C. M. N.; Anderson, A. S.; Aschenbrenner, L.; Avery, M.; Berritt, S.; Boras, B.; Cardin, R. D.; Carlo, A.; Coffman, K. J.; Dantonio, A.; Di, L.; Eng, H.; Ferre, R.; Gajiwala, K. S.; Gibson, S. A.; Greasley, S. E.; Hurst, B. L.; Kadar, E. P.; Kalgutkar, A. S.; Lee, J. C.; Lee, J.; Liu, W.; Mason, S. W.; Noell, S.; Novak, J. J.; Obach, R. S.; Ogilvie, K.; Patel, N. C.; Pettersson, M.; Rai, D. K.; Reese, M. R.; Sammons, M. F.; Sathish, J. G.; Singh, R. S. P.; Steppan, C. M.; Stewart, A. E.; Tuttle, J. B.; Updyke, L.; Verhoest, P. R.; Wei, L.; Yang, Q.; Zhu, Y. An oral SARS-CoV-2 M<sup>pro</sup> inhibitor clinical candidate for the treatment of COVID-19. *Science* **2021**, *374*, 1586–1593.

(26) Ullrich, S.; Ekanayake, K. B.; Otting, G.; Nitsche, C. Main protease mutants of SARS-CoV-2 variants remain susceptible to nirmatrelvir. *Bioorg. Med. Chem. Lett.* **2022**, *62*, 128629.

(27) Ashburn, T. T.; Thor, K. B. Drug repositioning: identifying and developing new uses for existing drugs. *Nat. Rev. Drug Discov.* **2004**, *3*, 673–683.

(28) Imran, M.; Alshrari, A. S.; Asdaq, S. M. B.; Abida. Trends in the development of remdesivir based inventions against COVID-19 and

other disorders: A patent review. *J. Infect. Public Health.* **2021**, *14*, 1075–1086.

(29) Painter, W. P.; Holman, W.; Bush, J. A.; Almazedi, F.; Malik, H.; Eraut, N. C. J. E.; Morin, M. J.; Szcwzyk, L. J.; Painter, G. R. Human Safety, Tolerability, and Pharmacokinetics of Molnupiravir, a Novel Broad-Spectrum Oral Antiviral Agent with Activity Against SARS-CoV-2. *Antimicrob. Agents Chemother.* **2021**, *65*, e02428–e02520.

(30) Gottlieb, R. L.; Vaca, C. E.; Paredes, R.; Mera, J.; Webb, B. J.; Perez, G.; Oguchi, G.; Ryan, P.; Nielsen, B. U.; Brown, M.; Hidalgo, A.; Sachdeva, Y.; Mittal, S.; Osiyemi, O.; Skarbinski, J.; Juneja, K.; Hyland, R. H.; Osinusi, A.; Chen, S.; Camus, G.; Abdelghany, M.; Davies, S.; Behenna-Renton, N.; Duff, F.; Marty, F. M.; Katz, M. J.; Ginde, A. A.; Brown, S. M.; Schiffer, J. T.; Hill, J. A. Early Remdesivir to Prevent Progression to Severe Covid-19 in Outpatients. *N. Engl. J. Med.* **2022**, *386*, 305–315.

(31) Fischer, W. A.; Eron, J. J.; Holman, W.; Cohen, M. S.; Fang, L.; Szcwzyk, L. J.; Sheahan, T. P.; Baric, R.; Mollan, K. R.; Wolfe, C. R.; Duke, E. R.; Azizad, M. M.; Borroto-Esoda, K.; Wohl, D. A.; Coombs, R. W.; James Loftis, A.; Alabanza, P.; Lipansky, F.; Painter, W. P. A phase 2a clinical trial of molnupiravir in patients with COVID-19 shows accelerated SARS-CoV-2 RNA clearance and elimination of infectious virus. *Sci. Transl. Med.* **2022**, *14*, No. eabl7430.

(32) Niknam, Z.; Jafari, A.; Golchin, A.; Danesh Pouya, F.; Nemati, M.; Rezaei-Tavirani, M.; Rasmi, Y. Potential therapeutic options for COVID-19: an update on current evidence. *Eur. J. Med. Res.* **2022**, *27*, 6.

(33) Cordillot, M.; Dubée, V.; Triboulet, S.; Dubost, L.; Marie, A.; Hugonnet, J. E.; Arthur, M.; Mainardi, J. L. In vitro cross-linking of Mycobacterium tuberculosis peptidoglycan by L,D-transpeptidases and inactivation of these enzymes by carbapenems. *Antimicrob. Agents Chemother.* **2013**, *57*, 5940–5945.

(34) Kumar, P.; Kaushik, A.; Lloyd, E. P.; Li, S. G.; Mattoo, R.; Ammerman, N. C.; Bell, D. T.; Perryman, A. L.; Zandi, T. A.; Ekins, S.; Ginell, S. L.; Townsend, C. A.; Freundlich, J. S.; Lamichhane, G. Non-classical transpeptidases yield insight into new antibacterials. *Nat. Chem. Biol.* **2017**, *13*, 54–61.

(35) Munnik, M.; Lohans, C. T.; Langley, G. W.; Bon, C.; Brem, J.; Schofield, C. J. A Fluorescence Based Assay for Screening  $\beta$  Lactams Targeting the Mycobacterium tuberculosis Transpeptidase Ldt<sub>Mt2</sub>. *Chembiochem* **2020**, *21*, 368–372.

(36) Steiner, E. M.; Schneider, G.; Schnell, R. Binding and processing of  $\beta$  lactam antibiotics by the transpeptidase Ldt<sub>Mt2</sub> from Mycobacterium tuberculosis. *FEBS J.* **2017**, *284*, 725–741.

(37) Malla, T. R.; Brewitz, L.; Muntean, D. G.; Aslam, H.; Owen, C. D.; Salah, E.; Tumber, A.; Lukacik, P.; Strain-Damerell, C.; Mikolajek, H.; Walsh, M. A.; Schofield, C. J. Penicillin Derivatives Inhibit the SARS-CoV-2 Main Protease by Reaction with Its Nucleophilic Cysteine. *J. Med. Chem.* **2022**, *65*, 7682–7696.

(38) Siddiqui, F.; Hoppensteadt, D.; Jeske, W.; Iqbal, O.; Tafur, A.; Fareed, J. Factor Xa Inhibitory Profile of Apixaban, Betrixaban, Edoxaban, and Rivaroxaban Does Not Fully Reflect Their Biologic Spectrum. *Clin. Appl. Thromb. Hemost.* **2019**, *25*, 1076029619847524.

(39) Foerster, K. I.; Hermann, S.; Mikus, G.; Haefeli, W. E. Correction to: Drug-Drug Interactions with Direct Oral Anticoagulants. *Clin. Pharmacokinet.* **2020**, *59*, 1647.

(40) Al-Horani, R. A. Potential Therapeutic Roles for Direct Factor Xa Inhibitors in Coronavirus Infections. *Am. J. Cardiovasc. Drugs* **2020**, *20*, 525–533.

(41) Bosch, F. T. M.; Candeloro, M.; Potere, N.; Porreca, E.; Di Nisio, M.; Kamphuisen, P. W. Effect of dexamethasone on direct Xa-inhibitor oral anticoagulant plasma levels in patients with COVID-19. *Thromb. Res.* **2021**, *205*, 106–109.

(42) Funk, E. A.; Strausbaugh, L. J. Antimicrobial activity, pharmacokinetics, adverse reactions, and therapeutic indications of cefoperazone. *Pharmacotherapy* **1982**, *2*, 185–196.

(43) Casapao, A. M.; Steed, M. E.; Levine, D. P.; Rybak, M. J. Ceftazolin fosamil for community-acquired bacterial pneumonia and

acute bacterial skin and skin structure infection. *Expet Opin. Pharmacother.* **2012**, *13*, 1177–1186.

(44) *Desmond Molecular Dynamics System*; D. E. Shaw Research: New York, NY, 2018.

(45) Lee, J.; Worrall, L. J.; Vuckovic, M.; Rosell, F. I.; Gentile, F.; Ton, A. T.; Caveney, N. A.; Ban, F.; Cherkasov, A.; Paetzel, M.; Strynadka, N. C. J. Crystallographic structure of wild-type SARS-CoV-2 main protease acyl-enzyme intermediate with physiological C-terminal autoprocessing site. *Nat. Commun.* **2020**, *11*, 5877.

(46) Sacco, M. D.; Hu, Y.; Gongora, M. V.; Meilleur, F.; Kemp, M. T.; Zhang, X.; Wang, J.; Chen, Y. The P132H mutation in the main protease of Omicron SARS-CoV-2 decreases thermal stability without compromising catalysis or small-molecule drug inhibition. *Cell Res.* **2022**, *32*, 498–500.

(47) Fact Sheet for Healthcare Providers. <https://www.fda.gov> (accessed December 2022).

(48) Gorog, D. A.; Storey, R. F.; Gurbel, P. A.; Tantry, U. S.; Berger, J. S.; Chan, M. Y.; Duerschmied, D.; Smyth, S. S.; Parker, W. A. E.; Ajjan, R. A.; Vilahur, G.; Badimon, L.; Berg, J. M. t.; Cate, H. t.; Peyvandi, F.; Wang, T. T.; Becker, R. C. Current and novel biomarkers of thrombotic risk in COVID-19: a Consensus Statement from the International COVID-19 Thrombosis Biomarkers Colloquium. *Nat. Rev. Cardiol.* **2022**, *19*, 475–495.

(49) Ranucci, M.; Sitzia, C.; Baryshnikova, E.; Di Dedda, U.; Cardani, R.; Martelli, F.; Corsi Romanelli, M. Covid-19-Associated Coagulopathy: Biomarkers of Thrombin Generation and Fibrinolysis Leading the Outcome. *J. Clin. Med.* **2020**, *9*, 3487.

(50) Beyer-Westendorf, J.; Verhamme, P.; Bauersachs, R. Betrixaban for prevention of venous thromboembolism in acute medically ill patients. *Eur. Heart J. Suppl.* **2018**, *20*, E16–E22.

(51) Huisman, M. V.; Klok, F. A. Pharmacological properties of betrixaban. *Eur. Heart J. Suppl.* **2018**, *20*, E12–E15.

(52) Kow, C. S.; Hasan, S. S. Pharmacologic therapeutic options for thromboprophylaxis in COVID-19. *J. Thromb. Thrombolysis* **2021**, *51*, 29–30.

(53) Lee, J. T.; Yang, Q.; Gribenko, A.; Perrin, B. S.; Zhu, Y.; Cardin, R.; Liberator, P. A.; Anderson, A. S.; Hao, L. Genetic Surveillance of SARS-CoV-2 M. *mBio* **2022**, *13*, No. e0086922.

(54) *Glide*; Schrödinger, LLC: New York, NY, 2018.

(55) *Protein Preparation Wizard*; Schrödinger, LLC: New York, NY, 2018.

(56) *MacroModel*; Schrödinger, LLC: New York, NY, 2018.

(57) Drugbank. [www.drugbank.ca](http://www.drugbank.ca) (accessed December 2022).

(58) *LigPrep*; Schrödinger, LLC: New York, NY, 2018.

(59) *Epik*; Schrödinger, LLC: New York, NY, 2018.

(60) ZINC15. <https://zinc15.docking.org/patterns/home> (accessed June 15, 2022).

(61) Pelliccia, S.; Cerchia, C.; Esposito, F.; Cannalire, R.; Corona, A.; Costanzi, E.; Kuzikov, M.; Gribbon, P.; Zaliani, A.; Brindisi, M.; Storici, P.; Tramontano, E.; Summa, V. Easy access to  $\alpha$ -ketoamides as SARS-CoV-2 and MERS Mpro inhibitors via the PADAM oxidation route. *Eur. J. Med. Chem.* **2022**, *244*, 114853.

(62) Costanzi, E.; Kuzikov, M.; Esposito, F.; Albani, S.; Demitri, N.; Giabbai, B.; Camasta, M.; Tramontano, E.; Rossetti, G.; Zaliani, A.; Storici, P. Structural and Biochemical Analysis of the Dual Inhibition of MG-132 against SARS-CoV-2 Main Protease (Mpro/3CLpro) and Human Cathepsin-L. *Int. J. Mol. Sci.* **2021**, *22*, 11779.

(63) Corona, A.; Wycisk, K.; Talarico, C.; Manelfi, C.; Milia, J.; Cannalire, R.; Esposito, F.; Gribbon, P.; Zaliani, A.; Iaconis, D.; Beccari, A. R.; Summa, V.; Nowotny, M.; Tramontano, E. Natural Compounds Inhibit SARS-CoV-2 nsp13 Unwinding and ATPase Enzyme Activities. *ACS Pharmacol. Transl. Sci.* **2022**, *5*, 226–239.

(64) Kuzikov, M.; Costanzi, E.; Reinshagen, J.; Esposito, F.; Vangeel, L.; Wolf, M.; Ellinger, B.; Claussen, C.; Geisslinger, G.; Corona, A.; Iaconis, D.; Talarico, C.; Manelfi, C.; Cannalire, R.; Rossetti, G.; Gossen, J.; Albani, S.; Musiani, F.; Herzog, K.; Ye, Y.; Giabbai, B.; Demitri, N.; Jochmans, D.; Jonghe, S. D.; Rymenants, J.; Summa, V.; Tramontano, E.; Beccari, A. R.; Leyssen, P.; Storici, P.; Neyts, J.; Gribbon, P.; Zaliani, A. Identification of Inhibitors of SARS-CoV-2

3CL-Pro Enzymatic Activity Using a Small Molecule in Vitro Repurposing Screen. *ACS Pharmacol. Transl. Sci.* **2021**, *4*, 1096–1110.

(65) Hu, Y.; Ma, C.; Szeto, T.; Hurst, B.; Tarbet, B.; Wang, J. Boceprevir, Calpain Inhibitors II and XII, and GC-376 Have Broad-Spectrum Antiviral Activity against Coronaviruses. *ACS Infect. Dis.* **2021**, *7*, 586–597.